Check for updates

Industrially viable formate production with 50% lower CO$_2$ emissions†

Fanxu Meng,‡[ad] Zihan Shen,‡[a] Xinlong Lin,‡[a] Pengfei Song,[a] Tianze Wu,[a] Shibo Xi,[e] Chao Wu,[e] Zhenhui Ma, [f] Daniel Mandler [*d] and Zhichuan J. Xu [*abc]

The conventional production of formic acid is energy-intensive, requiring methanol and carbon monoxide reactions followed by hydrolysis under high temperature and pressure. Methanol electrochemical refinery (e-refinery) offers a sustainable alternative but faces challenges like high overpotential and competing oxygen evolution reaction (OER). This study presents Pt-nanoparticle-decorated Ni(OH)$_2$ as a breakthrough catalyst, achieving a significantly lower onset potential of 0.5 V *vs.* reversible hydrogen electrode (RHE) for methanol-to-formate conversion compared to previous reports (>1.35 V *vs.* RHE), while simultaneously generating hydrogen at the cathode. The platinum valence state is identified as an effective descriptor for formate faradaic efficiency, validated through experimental studies and density functional theory. Pt$_{1.05}$@Ni(OH)$_2$, featuring the highest platinum valence states among the catalysts studied, exhibits an exceptional formate faradaic efficiency of 78.8% and a high formate production rate of 1.3 mmol h^{-1} mg$_{cat}^{-1}$ at 0.8 V *vs.* RHE. This approach reduces overpotential, eliminates OER, and cuts carbon dioxide emissions by over 50% compared to traditional methods. Moreover, economic analysis shows profitability from the fourth year at 50 mA cm^{-2}, supporting easier industrial adoption and low carbon dioxide emissions. These advancements offer a sustainable, energy-efficient, and economically viable method for formate production, advancing the commercialization of methanol e-refinery technology.

Broader context

A transition towards sustainable chemical production has driven a great interest into alternative methods that minimize environmental impact and energy consumption. Formic acid, a versatile chemical used in various industrial applications, is traditionally produced through energy-intensive processes involving methanol and carbon monoxide reactions. Such methods contribute significantly to carbon emissions and reliance on fossil fuels. Considering the future increase in green methanol production, the greener methods to produce formic acid from methanol is desired for a significant reduction in CO$_2$ emission of its supply chain. Electrochemical refinery of methanol to formate meets such a need due to its high electron-to-product efficiency. However, the high overpotential and competing OER have hindered its potential for practical implementation. This paper introduces a Pt-decorated Ni(OH)$_2$ catalyst that significantly achieves efficient and low-overpotential formate production with co-generation of hydrogen. It covers detailed studies on how the technique overcomes key technical barriers as well as the analysis of its economic and environmental benefits. The work marks a critical step toward the large-scale adoption of methanol e-refinery technology and its integration into a low-carbon economy.

[a] *School of Material Science and Engineering, Nanyang Technological University, 50 Nanyang Avenue, Singapore 639798, Singapore. E-mail: xuzc@ntu.edu.sg*

[b] *Energy Research Institute@Nanyang Technological University, ERI@N, Interdisciplinary Graduate School, Nanyang Technological University, 50 Nanyang Avenue, Singapore 639798, Singapore*

[c] *Center for Advanced Catalysis Science and Technology, Nanyang Technological University, 50 Nanyang Avenue, Singapore, 639798, Singapore*

[d] *Institute of Chemistry, The Hebrew University of Jerusalem, Jerusalem 9190401, Israel*

[e] *Institute of Sustainability for Chemicals, Energy, and Environment (ISCE2), Agency for Science, Technology and Research (A*STAR), 1 Pesek Road, Jurong Island, Singapore 627833, Singapore*

[f] *Department of Physics, Beijing Technology and Business University, Beijing 100048, China*

† Electronic supplementary information (ESI) available. See DOI: **https://doi.org/10.1039/d5ee00452g**

‡ These authors contributed equally to this work.

3680 | *Energy Environ. Sci.*, 2025, **18**, 3680–3688

This journal is © The Royal Society of Chemistry 2025

Introduction

Growing concerns regarding global warming and energy security have stimulated the advancement of carbon-neutral and sustainable technologies. Consequently, there is a pressing need to explore new sustainable pathways for the production of crucial platform chemicals and fuels, aiming to either interface or replace current petrochemical industries that heavily rely on fossil fuels with bio-derived feedstocks.[1–6] In this context, e-refinery processes have emerged as a promising option,[7–9] offering environmentally friendly and efficient solutions with precise control over reaction driving forces. This makes them particularly well-suited for optimizing partial oxidation or reduction reactions in the realm of sustainable chemical production.[10–14]

Methanol, characterized by its simplicity, ease of storage, and water solubility, can be industrially produced on a large scale from renewable bio-resources, making it a crucial industrial raw material for numerous chemicals. A significant portion, over 70%, of the global methanol production is allocated to chemical syntheses,[15] including the production of formic acid, dimethyl ether, and formaldehyde. Among these, formic acid stands out as a valuable chemical and a potential energy carrier, finding wide-ranging applications in industries such as textiles, printing, oil & gas, and aviation. However, the conventional process of producing formic acid from methanol involves the combination of methanol and carbon monoxide, followed by the hydrolysis of the resulting methyl formate under high temperature and pressure. This energy-intensive process results in formic acid being approximately twice as expensive as methanol.[16]

Upgrading the conventional fossil-fuel-based process with the e-refinery concept is imperative from both economic and environmental standpoints. However, the practical application of methanol e-refinery towards formate is currently hindered by its high overpotential. Existing catalysts, such as $Ni_{0.33}Co_{0.67}(OH)_2$,[17] $Co(OH)_2$,[18] $Ni_{0.75}Fe_{0.25}Se_2$,[19] $LaCo_{0.5}Fe_{0.5}O_3$,[20] $Ni(OH)_2$,[21] NiS,[22] and other transition metal catalysts,[23–41] operate at potentials mostly over 1.35 V vs. reversible hydrogen electrode (RHE). This potential greatly surpasses the theoretical potential of −0.06 V vs. standard hydrogen electrode (SHE) for the conversion: $CH_3OH + H_2O \rightarrow HCOOH + 4H^+ + 4e^-$. The theoretical potential is derived from two key equations: $CO_2 + 6H^+ + 6e^- \rightarrow CH_3OH(aq) + H_2O$, $E^0 = 0.016$ V vs. SHE[42] and $CO_2 + 2H^+ + 2e^- \rightarrow HCOOH$, $E^0 = -0.07$ V vs. SHE.[43] Although catalysts such as Pt[44] and PtRu[45] have succeeded in lowering the overpotential of methanol oxidation to around 0.6 V vs. RHE, their focus on fully oxidizing methanol to CO_2/carbonate[46–48] renders them unsuitable for the mild methanol-to-formate e-refinery process.

This study overcomes those limitations by significantly reducing the onset potential of the methanol e-refinery to approximately 0.5 V vs. RHE with Pt decorated $Ni(OH)_2$. Methanol oxidation on platinum (Pt) is well-known to proceed via a dual-pathway mechanism, with the indirect CO_{ad} pathway dominating below 0.65 V vs. RHE, while the direct H_xCO_{ad} pathway becomes prominent above 0.7 V vs. RHE.[49–52] This shift aligns well with the onset of OH adsorption peaks on Pt,[53] after which the valence states of surface Pt atoms increase. In this study, Pt nanoparticles are combined with $Ni(OH)_2$, where the heterojunction between Pt and $Ni(OH)_2$ elevates Pt valence states, which, in turn, correlate positively with formate faradaic efficiency. This innovative discovery is substantiated through the examination of additional catalysts as well as theoretical computations. Among the catalysts scrutinized, $Pt_{1.05}@Ni(OH)_2$, characterized by the highest Pt valence states, showcases an outstanding formate faradaic efficiency of 78.8% and a notable formate production rate of 1.3 mmol h^{-1} mg_{cat}^{-1} at 0.8 V vs. RHE. Importantly, the reduction in operating potential eliminates competing OER, thus enhancing formate production efficiency and significantly lowering energy consumption and carbon dioxide emissions. Since methanol plays critical roles in advanced chemical production and hydrogen storage/transportation, this work constitutes a substantial advancement in the methanol economy and decarbonization of chemical industry.
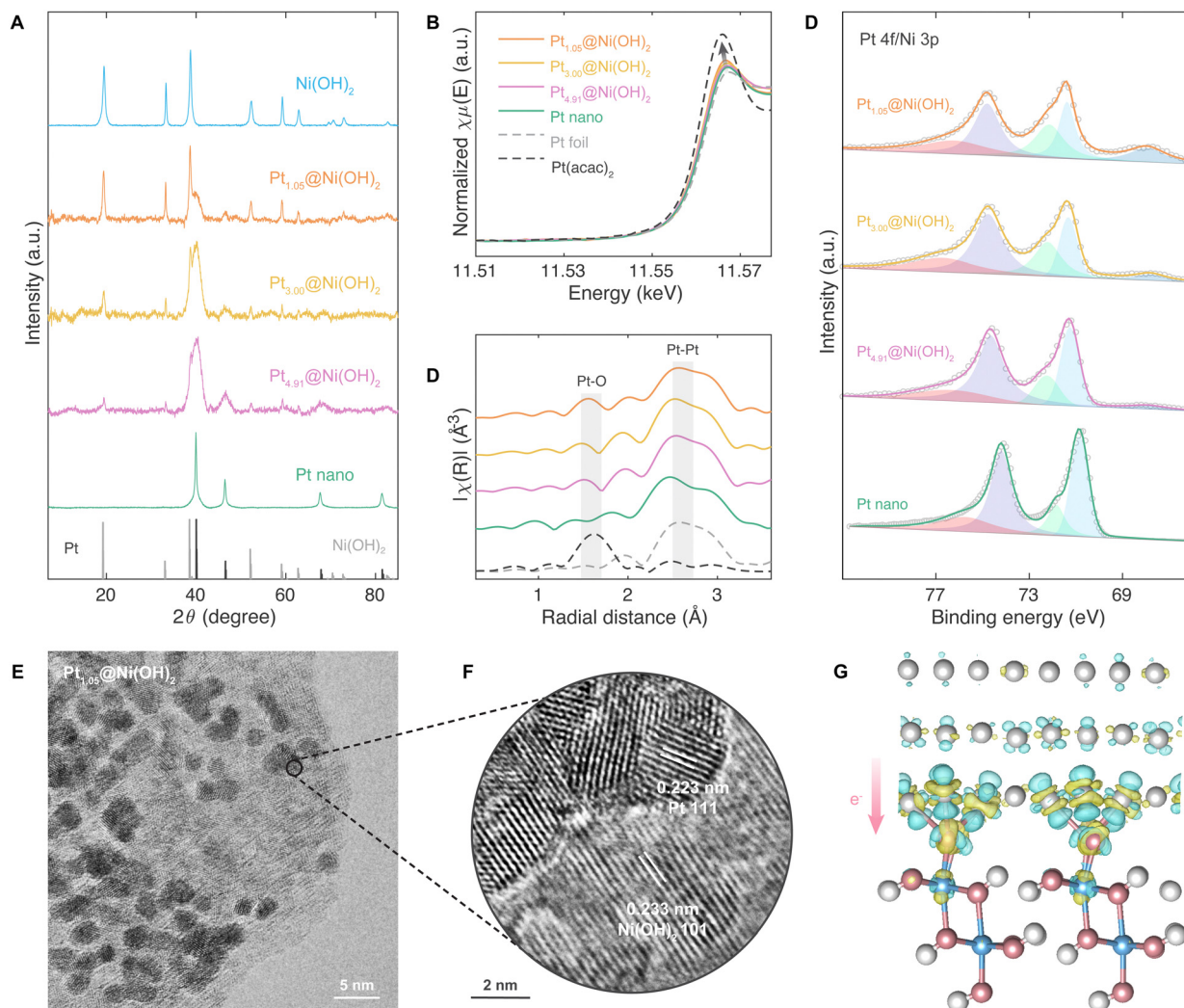
Results and discussion

Material characterization

After synthesis, all catalysts undergo inductively coupled plasma mass spectrometry (ICP-MS) testing to determine the Pt and Ni molar ratio. The catalysts are named based on the molar ratio between Pt and Ni, with Ni calibrated to 1 (refer to ESI,† Table S1).

To elucidate the crystallographic properties of the catalysts, X-ray diffraction (XRD) analysis is performed, as depicted in Fig. 1a. The XRD pattern of commercial $Ni(OH)_2$ and Pt nano matches $Ni(OH)_2$ $P\bar{3}m1$ (164) and Pt $Fm\bar{3}m$ (225), respectively, with no impurity peaks detected. As the Pt decoration ratio increases, the Pt diffraction peak gradually rises, indicating an increase in Pt content in the catalyst. The local atomic and electronic structures of the catalysts are examined using X-ray absorption near-edge structure (XANES), extended X-ray absorption fine structure (EXAFS), and X-ray photoelectron spectroscopy (XPS) (refer to Fig. 1b–d and Fig. S1, S2, ESI†). According to the XANES figure, the Pt valence states in $Pt_x@Ni(OH)_2$ gradually increase with decreasing Pt content, though the majority of Pt nanoparticles remain metallic, as evidenced by the strong Pt–Pt bond and weak Pt–O bond in Fig. 1c. This observation is corroborated by the XPS plots, where the binding energy increases gradually with decreasing Pt content, indicating a corresponding increase in Pt valence states. The peaks observed at around 856.3 eV, 873.8 eV, 67.9 eV, 71.4 eV, 72.1 eV, 74.8 eV, 76.8 eV, 531.3 eV, and 532.3 eV are attributed to Ni $2p_{3/2}$, Ni $2p_{1/2}$, Ni $3p_{3/2}$, Pt^0 $4f_{7/2}$, Pt^{+2} $4f_{7/2}$, Pt^0 $4f_{5/2}$, Pt^{+2} $4f_{5/2}$, O in Ni–O, and O in adsorbed H_2O, respectively.[54–57] High-resolution transmission electron microscopy (HRTEM) images of the catalysts are shown in Fig. 1e and f and Fig. S3, S4 (ESI†). The images reveal that Pt nanocrystals (dark particles) exhibit a diameter of approximately 2–4 nm, and the particle density increases gradually with the Pt/Ni ratio. Fig. 1g presents the charge density difference of the Pt–$Ni(OH)_2$ heterojunction calculated using density functional theory (DFT), where a heterojunction is established between the $Ni(OH)_2(101)$ face and Pt(111) face, as

This journal is © The Royal Society of Chemistry 2025

Energy Environ. Sci., 2025, **18**, 3680–3688 | **3681**

Fig. 1 Characterizations of $Pt_x@Ni(OH)_2$ (x = 0.00, 1.05, 3.00, and 4.91) and Pt nano. (a) XRD, (b) XANES, (c) EXAFS, and (d) XPS spectra for $Pt_x@Ni(OH)_2$ (x = 0.00, 1.05, 3.00, and 4.91) and Pt nano. (e) and (f) HRTEM images of $Pt_{1.05}@Ni(OH)_2$. (g) Charge density difference of $Pt–Ni(OH)_2$ heterojunction. The cyan regions indicate charge depletion, while the yellow regions represent charge accumulation, with an isosurface value of 0.01 e $Å^{-3}$.

observed in the HRTEM figures in Fig. 1f and Fig. S4 (ESI†). Self-consistent calculations have confirmed the charge-deficient status of the Pt layer, thereby validating the experimental findings from a theoretical perspective.
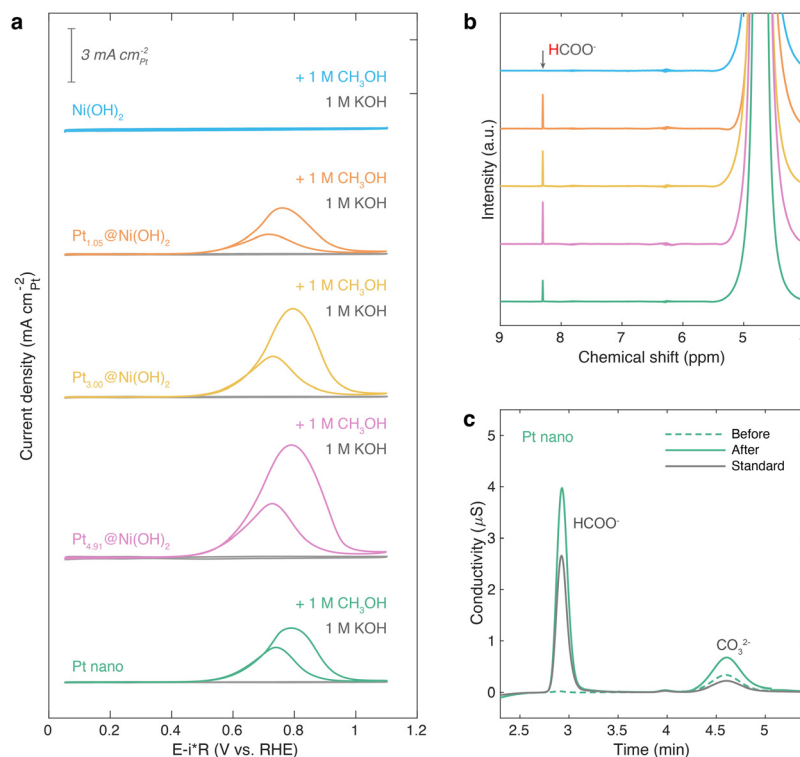
Methanol e-refinery performance

To assess the performance of $Pt_x@Ni(OH)_2$ and Pt nano in methanol e-refinery processes, cyclic voltammetry (CV) and chronoamperometry (CA) experiments at 0.8 V *vs.* RHE are conducted using the five electrocatalysts in a typical H-type electrochemical cell. The cell comprises distinct anode and cathode compartments. In the cathodic chamber, a platinum plate (1×2 cm^2) functions as the counter electrode, facilitating the hydrogen evolution reaction (HER). Within the anodic chamber, a Hg/HgO electrode serves as the reference electrode, while a catalyst-modified glassy carbon electrode acts as the working electrode, where the electrochemical conversion of methanol takes place. Following electrochemical testing, nuclear magnetic resonance

(NMR) and ion chromatography (IC), analyses are carried out to identify potential reaction products. Fig. 2a displays the CV curves for each electrocatalyst, revealing that an increase in Pt content is accompanied by a corresponding increase in the methanol oxidation peak for $Pt_x@Ni(OH)_2$ (x = 0.00, 1.05, 3.00, and 4.91). A representative CA profile for $Pt_{1.05}@Ni(OH)_2$ is presented in Fig. S5 (ESI†). In Fig. 2b, NMR spectra for the five catalysts show a gradual increase in the peak[58] corresponding to HCOO$^-$ as the catalyst transitions from $Ni(OH)_2$ to $Pt_{4.91}@Ni(OH)_2$. HCHO, located around 4.4 ppm,[59] is not observed, indicating its absence in the methanol e-refinery products. Fig. 2c presents the IC curves for Pt nano, with peaks at 2.9 min and 4.6 min attributed to HCOO$^-$ and CO$_3^{2-}$, respectively, suggesting the production of abundant HCOO$^-$ and CO$_3^{2-}$ on Pt nano.

Fig. 3a and b provide a summary of the formate production rate and faradaic efficiency after 2-hour CA test at 0.8 V *vs.* RHE. Two notable observations emerge from these figures. Firstly, $Ni(OH)_2$ fails to activate methanol at 0.8 V *vs.* RHE. Secondly,

3682 | *Energy Environ. Sci.*, 2025, **18**, 3680–3688

This journal is © The Royal Society of Chemistry 2025

Fig. 2 Electrochemical performances of $Pt_x@Ni(OH)_2$ (x = 0.00, 1.05, 3.00, and 4.91) and Pt nano. (a) CV profiles in 1 M KOH + 1 M CH_3OH in comparison with 1 M KOH on $Pt_x@Ni(OH)_2$ (x = 0.00, 1.05, 3.00, and 4.91) and Pt nano. (b) NMR spectra of the five catalysts. The positions for $HCOO^-$ and HCHO are around 8.3 ppm and 4.4 ppm,[58,59] respectively. No peaks for HCHO are observed for all catalysts. (c) IC patterns of Pt nano. To counteract CO_2 adsorption from open air, IC tests are conducted before and after the CA experiments.

the formate production rate increases with the Pt ratio on $Pt_x@Ni(OH)_2$ (x = 1.05, 3.00, and 4.91), albeit with a gradual decrease in faradaic efficiency. The first observation aligns with the CV curves depicted in Fig. 2a, indicating $Ni(OH)_2$'s incapacity to convert methanol at 0.8 V vs. RHE. The slight enhancement in formate production rate in the second observation results from the increase in Pt content among $Pt_x@Ni(OH)_2$ (x = 1.05, 3.00, and 4.91). In contrast, the variation in formate faradaic efficiency is attributed to the heightened valence states

of $Pt_x@Ni(OH)_2$ (x = 1.05, 3.00, and 4.91), as evidenced by the X-ray absorption spectroscopy (XAS) and XPS curves presented in Fig. 1b–d, indicating its potential capability as an efficient descriptor for methanol-to-formate faradaic efficiencies. Additionally, Fig. 3c compares the onset potential and formate faradaic efficiency of $Pt_{1.05}@Ni(OH)_2$ with other methanol e-refinery catalysts reported in the literature, highlighting the significantly lower operation potential of $Pt_{1.05}@Ni(OH)_2$ compared to previous findings.[17–21]
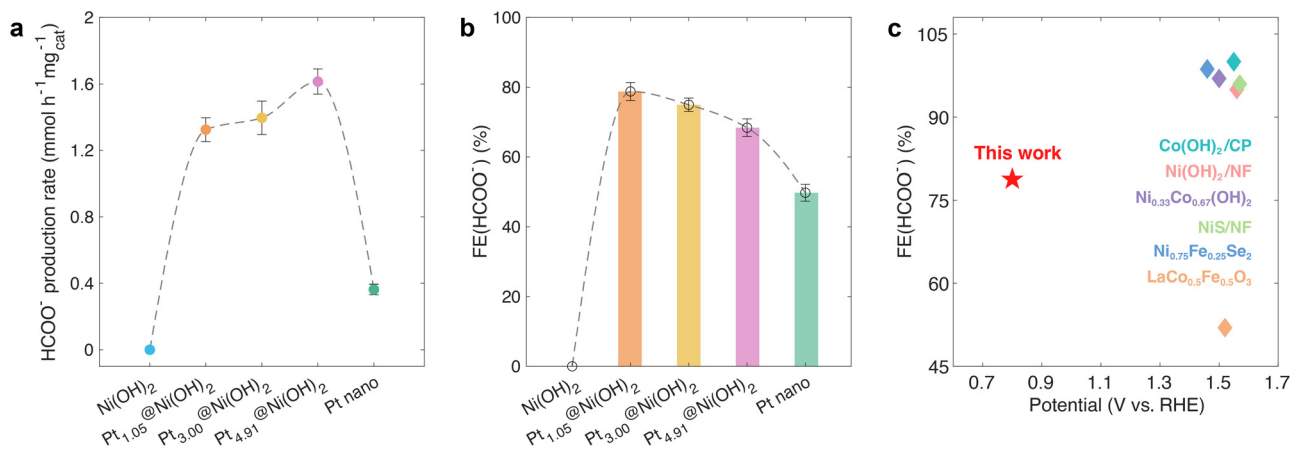
Fig. 3 Methanol e-refinery product analysis of $Pt_x@Ni(OH)_2$ (x = 0.00, 1.05, 3.00, and 4.91) and Pt nano. (a) Formate production rate and (b) faradaic efficiency. (c) Performance comparison between $Pt_{1.05}@Ni(OH)_2$ and other methanol e-refinery catalysts in the literature.

This journal is © The Royal Society of Chemistry 2025

Energy Environ. Sci., 2025, **18**, 3680–3688 | **3683**

Methanol e-refinery mechanisms

Fig. 4a clearly illustrates the direct relationship between formate faradaic efficiency and the Pt $4f_{5/2}$ energy, which is an indicator of Pt valence states, showing a near-linear relationship. Similarly, Fig. S6a and c (ESI†) depicts the relationships between formate faradaic efficiency and both the Pt $4f_{7/2}$ binding energy and the white-line intensity in XANES analysis, respectively, both of which display comparable proportional dependencies. Fig. 4b systematically illustrates this phenomenon. Furthermore, the energy variations of the methanol e-refinery reaction on Pt-loaded $Ni(OH)_2$ and pure Pt nanoparticles are calculated to better illustrate the correlation between Pt valence states and formate faradaic efficiency. The reaction route follows previous literature reports:[45,48–52,60] the first three steps are methanol deprotonation processes, forming a *CHO intermediate, followed by two hydroxide-attacking steps to produce $HCOO^-$ (refer to Fig. 4c). The energy profiles of $Pt@Ni(OH)_2$ compared to pristine Pt nanoparticles have also been delineated in Fig. 4c. Notably, the $Pt@Ni(OH)_2$ demonstrates a diminished energy barrier for the rate-limiting step, corroborating the beneficial influence of the elevated valence state of platinum on the catalytic conversion of methanol to formate.

Moreover, to further substantiate the relationship between Pt valence states and formate production from methanol, a 5-minute methanol e-refinery reaction at 0.8 V *vs.* RHE is conducted on $Pt_{1.05}@Ni(OH)_2$ following a 5-minute HER in

1 M KOH at -0.1 V *vs.* RHE. This process is repeated 24 times successively, resulting in a total methanol e-refinery time of 2 hours. The formate faradaic efficiency exhibits a decrease to approximately 60.0% (Fig. S7, ESI†) compared to that of $Pt_{1.05}@Ni(OH)_2$ in Fig. 3b, thus reinforcing the correlation between Pt valence states and formate faradaic efficiency. Additionally, the formate faradaic efficiency is examined for Pt nanoparticles loaded on $Co(OH)_2$ under identical CA conditions, as shown in Fig. S8 (ESI†). $Pt@Co(OH)_2$ demonstrates a noteworthy formate faradaic efficiency of approximately 77.0%. The results from both experiments provide further evidence supporting the wide applicability and effectiveness of the Pt-valence-state descriptor for the methanol e-refinery process.

MEA membrane electrode assembly test

Leveraging the promising properties of $Pt_{1.05}@Ni(OH)_2$, this anode is incorporated into a 2×2 cm² membrane electrode assembly (MEA) cell configuration, as detailed in a prior study.[20] The MEA cell, schematically represented in Fig. 5a, features an anion exchange membrane (AEM) that segregates the cathode and anode compartments. In this setup, $Pt_{1.05}@Ni(OH)_2$ (2 mg cm^{-2}) serves as the anode catalyst, while commercial Pt/C (1 mg cm^{-2}) is employed as the cathode catalyst.

To assess the electrochemical performance of the catalyst, polarization results are generated by performing a 3-minute
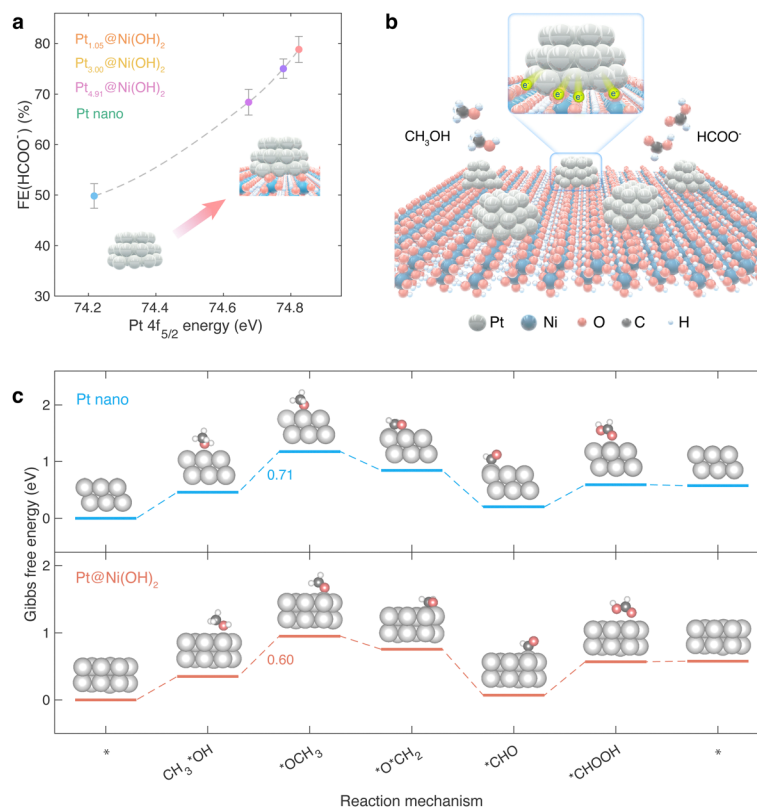

Fig. 4 Methanol e-refinery mechanisms towards formate. (a) The relationship between Pt $4f_{5/2}$ energy and formate faradaic efficiencies of $Pt_x@Ni(OH)_2$ (x = 1.05, 3.00, and 4.91) and Pt nano. (b) The reaction diagram of methanol e-refinery on Pt-loaded $Ni(OH)_2$. (c) Possible reaction route and the corresponding computed free energy changes of methanol e-refinery towards formate on Pt and Pt-loaded $Ni(OH)_2$.

3684 | *Energy Environ. Sci.*, 2025, **18**, 3680–3688

This journal is © The Royal Society of Chemistry 2025
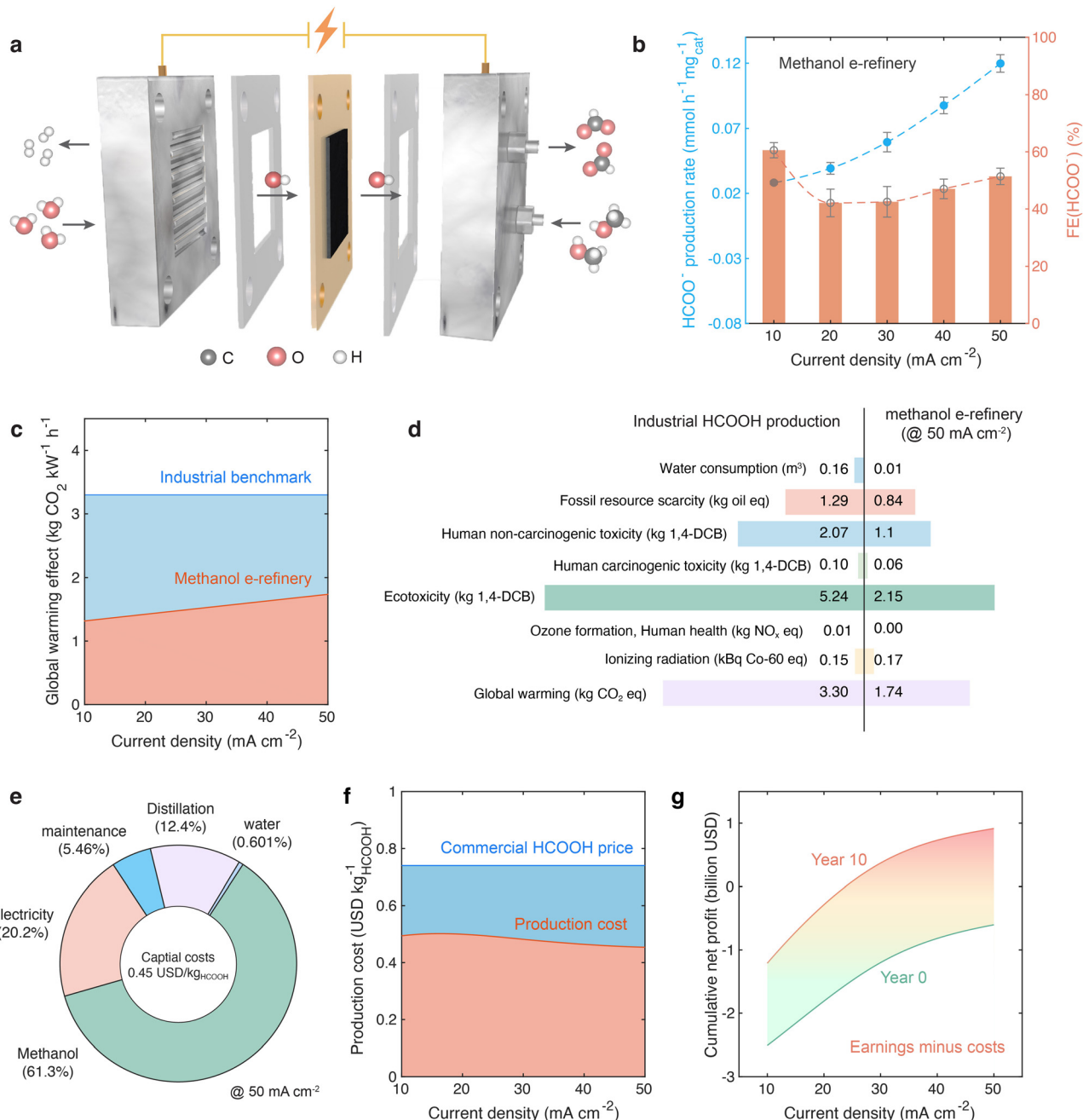
Fig. 5 MEA test on $Pt_{1.05}@Ni(OH)_2$. (a) Schematic diagram for the methanol e-refinery MEA cell. (b) $HCOO^-$ production rates and faradaic efficiencies at 10, 20, 30, 40, and 50 mA cm^{-2} in 1 M KOH + 1 M CH_3OH. (c) Comparative analysis of global warming impacts for the methanol e-refinery MEA cell vs. industrial formic acid production at 10, 20, 30, 40, and 50 mA cm^{-2}. (d) Detailed environmental impact assessment of the methanol e-refinery MEA cell compared to industrial formic acid production. (e) Cost analysis for the methanol e-refinery MEA cell. (f) Comparative evaluation of production costs for the methanol e-refinery MEA cell vs. the commercial formic acid price. (g) Cumulative net profit analysis for the methanol e-refinery MEA cell plant.

chronopotentiometry (CP) test for both 1 M KOH + 1 M CH_3OH and 1 M KOH electrolytes at current densities of 10, 20, 30, 40, and 50 mA cm^{-2} (geometric area), a temperature of 80 °C, and an electrolyte flow rate of 2 ml min^{-1}. Notably, the methanol e-refinery reaction exhibited a considerably lower potential compared to OER on $Pt_{1.05}@Ni(OH)_2$ at a fixed current density, as depicted in Fig. S9a (ESI†).

Following the polarization experiments, a 30-minute CP test is conducted at current densities of 10, 20, 30, 40, and 50 mA cm^{-2} (geometric area) in 1 M KOH + 1 M CH_3OH, as presented in Fig. S9b (ESI†). The electrolytes are subsequently analyzed by IC to quantify the concentration of formate ions ($HCOO^-$). Fig. 5b illustrates the production rate and faradaic efficiency of $HCOO^-$. Notably, formate faradaic efficiency takes a considerable share at all current densities.

This journal is © The Royal Society of Chemistry 2025

Energy Environ. Sci., 2025, **18**, 3680–3688 | **3685**

To comprehensively elucidate the advantages of the methanol e-refinery MEA design, both environmental impact and economic profit analyses are conducted. The environmental impact, quantified in terms of equivalent carbon dioxide emissions, of the MEA cell is evaluated through a life cycle assessment (LCA). This assessment is compared with the conventional method of formic acid production *via* the combination of methanol and carbon monoxide followed by methyl formate hydrolysis.[61–64] The LCA is conducted in accordance with the ISO 14040 and 14044 frameworks (additional details are provided in the ESI†). During the calculations, all mass and energy inputs and outputs associated with formic acid production are considered, encompassing a cradle-to-gate approach. As illustrated in Fig. 5c, the carbon dioxide emissions of methanol e-refinery cell are less than half of the conventional industrial process at 10–40 mA cm^{-2} and approximately half at 50 mA cm^{-2}. Beyond CO$_2$ emissions, the methanol e-refinery cell demonstrates superior performance across all other environmental impact metrics compared to the conventional process at 50 mA cm^{-2}, as shown in Fig. 5d. The economic assessment takes into account various factors, including reactant and electricity consumption, distillation costs, machine operation and maintenance expenses, and other practical considerations.[65–67] The prices of H$_2$,[68] CH$_3$OH,[69] HCOOH,[70] and electricity[71] are set at 1.26 USD kg^{-1}, 0.40 USD kg^{-1}, 0.74 USD kg^{-1}, and 0.03 USD kW^{-1} h^{-1}, respectively. Fig. 5e systematically presents the formic acid production cost of the methanol e-refinery cell at 50 mA cm^{-2}, and Fig. 5f compares the production cost to the commercial formic acid price. The formic acid produced by this method shows a significant cost advantage over the commercially available formic acid. However, when taking into account the practical factors required for establishing a new plant–such as the initial investments in plant construction, the installation of electrolyzer stacks, and the purchase of distillation equipment–the cumulative net profit (defined as total earnings minus total costs, as shown in Fig. 5g) is negative during the first year. Nevertheless, with continuous catalyst refreshment and equipment maintenance (costs of which are included in the calculation), the plant is projected to achieve positive cumulative net profits since the fourth year at a current density of 50 mA cm^{-2} (Fig. 5g). If the current density increases, with the concomitant increase of energy consumption and carbon dioxide emissions, the time required to attain positive cumulative net profits can be shortened to twenty-five months at 100 mA cm^{-2}, thirteen months at 200 mA cm^{-2}, and ten months at 300 mA cm^{-2} (Fig. S10, ESI†). However, a high current density is technically challenging to achieve in a MEA system, accompanied with higher capital investment, more carbon dioxide emissions, and lower energy efficiency. A low current density like 50 mA cm^{-2} can be readily achieved and managed by current MEA techniques. Detailed calculation methods for the cumulative net profit of the methanol e-refinery MEA cell are provided in the ESI.†

Conclusions

The strategic incorporation of platinum nanoparticles onto Ni(OH)$_2$ substrates has been demonstrated to effectively modulate the electronic states of platinum. Both experimental and theoretical evidence presented here demonstrate, for the first time, a direct correlation between the valence states of platinum and formate faradaic efficiency for the methanol e-refinery reaction. Pt$_{1.05}$@Ni(OH)$_2$, which exhibits the highest platinum valence states among the catalysts studied, achieves an exceptional formate faradaic efficiency of 78.8% and a low onset potential of approximately 0.5 V *vs.* RHE, effectively mitigating the competition from OER. The decrease in overpotential and the concomitant elimination of OER translate into a significant decrease in both carbon dioxide emissions and energy consumption in the methanol e-refinery MEA setup, with a projected CO$_2$ emissions reduction of over 50% compared to the conventional formic acid production process. Furthermore, the process achieves positive cumulative net profits beginning in the fourth year at a current density of 50 mA cm^{-2}, showcasing a combination of low carbon dioxide emissions, high energy efficiency, and substantial economic profitability. These findings underscore the novelty and impact of this work, highlighting a critical advancement in the scalability and feasibility of methanol electrochemical refinery technology. By addressing key challenges in efficiency and environmental impact, this study paves the way for the adoption of methanol e-refinery in commercial applications, offering a sustainable and economically viable alternative for formic acid production.

Author contributions

F. M., Z. J. X., and D. M. designed the experiments. F. M. performed the experiments, analyzed the data and wrote the draft manuscript. Z. S. did the DFT calculations. X. L. helped with the MEA and LCA analysis. P. S. helped with the TEM measurements. S. X. and C. W. helped with the XAS measurements. Z. M. helped with the TEA analysis. F. M. and Z. J. Xu. helped with the draft manuscript preparation.

Data availability

The data that support the findings in this study are available from the corresponding author upon reasonable request.

Conflicts of interest

There are no conflicts to declare.

Acknowledgements

3686 | Energy Environ. Sci., 2025, 18, 3680–3688

This journal is © The Royal Society of Chemistry 2025

References

1 W. F. Lamb, T. Wiedmann, J. Pongratz, R. Andrew, M. Crippa, J. G. J. Olivier, D. Wiedenhofer, G. Mattioli, A. A. Khourdajie, J. House, S. Pachauri, M. Figueroa, Y. Saheb, R. Slade, K. Hubacek, L. Sun, S. K. Ribeiro, S. Khennas, S. de la Rue du Can, L. Chapungu, S. J. Davis, I. Bashmakov, H. Dai, S. Dhakal, X. Tan, Y. Geng, B. Gu and J. Minx, *Environ. Res. Lett.*, 2021, **16**, 073005.

2 P. De Luna, C. Hahn, D. Higgins, S. A. Jaffer, T. F. Jaramillo and E. H. Sargent, *Science*, 2019, **364**, eaav3506.

3 S. Mou, T. Wu, J. Xie, Y. Zhang, L. Ji, H. Huang, T. Wang, Y. Luo, X. Xiong, B. Tang and X. Sun, *Adv. Mater.*, 2019, **31**, 1903499.

4 L. Ji, L. Li, X. Ji, Y. Zhang, S. Mou, T. Wu, Q. Liu, B. Li, X. Zhu, Y. Luo, X. Shi, A. M. Asiri and X. Sun, *Angew. Chem., Int. Ed.*, 2020, **59**, 758–762.

5 T. Ahmad, S. Liu, M. Sajid, K. Li, M. Ali, L. Liu and W. Chen, *Nano Res. Energy*, 2022, **1**, 9120021.

6 L. Li, I. M. U. Hasan, Farwa, R. He, L. Peng, N. Xu, N. K. Niazi, J.-N. Zhang and J. Qiao, *Nano Res. Energy*, 2022, **1**, 9120015.

7 B. S. Crandall, B. H. Ko, S. Overa, L. Cherniack, A. Lee, I. Minnie and F. Jiao, *Nat. Chem. Eng.*, 2024, **1**, 421–429.

8 J. Lee, S. M. Kim, B. W. Jeon, H. W. Hwang, E. G. Poloniataki, J. Kang, S. Lee, H. W. Ra, J. Na, J.-G. Na, J. Lee and Y. H. Kim, *Nat. Chem. Eng.*, 2024, **1**, 354–364.

9 Z. Li, P. Wang, X. Lyu, V. K. R. Kondapalli, S. Xiang, J. D. Jimenez, L. Ma, T. Ito, T. Zhang, J. Raj, Y. Fang, Y. Bai, J. Li, A. Serov, V. Shanov, A. I. Frenkel, S. D. Senanayake, S. Yang, T. P. Senftle and J. Wu, *Nat. Chem. Eng.*, 2024, **1**, 159–169.

10 J. E. Huang, Y. Chen, P. Ou, X. Ding, Y. Yan, R. Dorakhan, Y. Lum, X.-Y. Li, Y. Bai, C. Wu, M. Fan, M. G. Lee, R. K. Miao, Y. Liu, C. O'Brien, J. Zhang, C. Tian, Y. Liang, Y. Xu, M. Luo, D. Sinton and E. H. Sargent, *J. Am. Chem. Soc.*, 2024, **146**, 8641–8649.

11 E. Shirzadi, Q. Jin, A. S. Zeraati, R. Dorakhan, T. J. Goncalves, J. Abed, B.-H. Lee, A. S. Rasouli, J. Wicks, J. Zhang, P. Ou, V. Boureau, S. Park, W. Ni, G. Lee, C. Tian, D. M. Meira, D. Sinton, S. Siahrostami and E. H. Sargent, *Nat. Commun.*, 2024, **15**, 2995.

12 X. Wang, Y. Chen, F. Li, R. K. Miao, J. E. Huang, Z. Zhao, X.-Y. Li, R. Dorakhan, S. Chu, J. Wu, S. Zheng, W. Ni, D. Kim, S. Park, Y. Liang, A. Ozden, P. Ou, Y. Hou, D. Sinton and E. H. Sargent, *Nat. Commun.*, 2024, **15**, 616.

13 X. Wang, P. Li, J. Tam, J. Y. Howe, C. P. O'Brien, A. Sedighian Rasouli, R. K. Miao, Y. Liu, A. Ozden, K. Xie, J. Wu, D. Sinton and E. H. Sargent, *Nat. Sustainability*, 2024, **7**, 931–937.

14 Y. Liang, F. Li, R. K. Miao, S. Hu, W. Ni, S. Zhang, Y. Liu, Y. Bai, H. Wan, P. Ou, X.-Y. Li, N. Wang, S. Park, F. Li, J. Zeng, D. Sinton and E. H. Sargent, *Nat. Synth.*, 2024, **3**, 1104–1112.

15 J. Ott, V. Gronemann, F. Pontzen, E. Fiedler, G. Grossmann, D. B. Kersebohm, G. Weiss and C. Witte, *Methanol, Ullmann's Encyclopedia of Industrial Chemistry,* Wiley-VCH, Weinheim, Germany, 2012.

16 P. Gautam, Neha, S. N. Upadhyay and S. K. Dubey, *Fuel*, 2020, **273**, 117783.

17 M. Li, X. Deng, K. Xiang, Y. Liang, B. Zhao, J. Hao, J. L. Luo and X. Z. Fu, *ChemSusChem*, 2020, **13**, 914–921.

18 K. Xiang, D. Wu, X. Deng, M. Li, S. Chen, P. Hao, X. Guo, J. L. Luo and X. Z. Fu, *Adv. Funct. Mater.*, 2020, **30**, 1909610.

19 J. Li, C. Xing, Y. Zhang, T. Zhang, M. C. Spadaro, Q. Wu, Y. Yi, S. He, J. Llorca, J. Arbiol, A. Cabot and C. Cui, *Small*, 2021, **17**, e2006623.

20 F. Meng, C. Dai, Z. Liu, S. Luo, J. Ge, Y. Duan, G. Chen, C. Wei, R. R. Chen, J. Wang, D. Mandler and Z. J. Xu, *eScience*, 2022, **2**(1), 87–94.

21 J. Hao, J. Liu, D. Wu, M. Chen, Y. Liang, Q. Wang, L. Wang, X.-Z. Fu and J.-L. Luo, *Appl. Catal., B*, 2021, **281**, 119510.

22 Z. Pi and H. Zhong, *IOP Conf. Ser. Earth Environ. Sci.*, 2021, **651**, 042062.

23 M. I. Abdullah, A. Hameed, N. Zhang, M. H. Islam, M. Ma and B. G. Pollet, *ACS Appl. Mater. Interfaces*, 2021, **13**, 30603–30613.

24 A. A. Dubale, Y. Zheng, H. Wang, R. Hübner, Y. Li, J. Yang, J. Zhang, N. K. Sethi, L. He, Z. Zheng and W. Liu, *Angew. Chem., Int. Ed.*, 2020, **59**, 13891–13899.

25 S.-N. Sun, L.-Z. Dong, J.-R. Li, J.-W. Shi, J. Liu, Y.-R. Wang, Q. Huang and Y.-Q. Lan, *Angew. Chem., Int. Ed.*, 2022, **61**, e202207282.

26 Y. Fan, X. Yang, E. Wei, Y. Dong, H. Gao, X. Luo and W. Yang, *Appl. Catal., B*, 2024, **345**, 123716.

27 Y. Xu, M. Liu, M. Wang, T. Ren, K. Ren, Z. Wang, X. Li, L. Wang and H. Wang, *Appl. Catal., B*, 2022, **300**, 120753.

28 B. Neppolian, *Ceram. Int.*, 2022, **48**, 29025–29030.

29 J. Chen, M. Ahmad, Y. Zhang, H. Ye, L. Wang, J. Zhang, X.-Z. Fu and J.-L. Luo, *J. Chem. Eng.*, 2023, **454**, 140056.

30 Y. Hao, D. Yu, S. Zhu, C.-H. Kuo, Y.-M. Chang, L. Wang, H.-Y. Chen, M. Shao and S. Peng, *Energy Environ. Sci.*, 2023, **16**, 1100–1110.

31 Y. Lin, Y.-g Wang, X. Li, J. Zhao, H. Liu, C. Wu, L. Yang, G. Li, Z. Qi, L. Shan, Y. Jiang and L. Song, *Small*, 2024, **20**, 2311452.

32 Y. Tong, X. Yan, J. Liang and S. X. Dou, *Small*, 2021, **17**, 1904126.

33 Y. Qi, Y. Zhang, L. Yang, Y. Zhao, Y. Zhu, H. Jiang and C. Li, *Nat. Commun.*, 2022, **13**, 4602.

34 B. Zhu, B. Dong, F. Wang, Q. Yang, Y. He, C. Zhang, P. Jin and L. Feng, *Nat. Commun.*, 2023, **14**, 1686.

35 N. T. R. Kumar, S. Kamalakannan, M. Prakash, B. Viswanathan and B. Neppolian, *ACS Appl. Energy Mater.*, 2022, **5**, 2104–2111.

36 Z. Li, Y. Gao, X. Meng, B. Sun, K. Song, Z. Wang, Y. Liu, Z. Zheng, P. Wang, Y. Dai, H. Cheng and B. Huang, *Cell Rep.*, 2022, **3**, 100972.

37 J. Zhang, Y. Hua, H. Li, X. Zhang, C. Shi, Y. Li, L. Di and Z. Wang, *J. Chem. Eng.*, 2023, **478**, 147288.

38 L. Zhao, Q. Sun, M. Li, Y. Zhong, P. Shen, Y. Lin and K. Xu, *Sci. China Mater.*, 2023, **66**, 1820–1828.

39 M. Khan, M. I. Abdullah, A. Samad, Z. Shao, T. Mushiana, A. Akhtar, A. Hameed, N. Zhang, U. Schwingenschlögl and M. Ma, *Small*, 2023, **19**, 2205499.

This journal is © The Royal Society of Chemistry 2025

Energy Environ. Sci., 2025, **18**, 3680–3688 | **3687**

40 F. Meng, Q. Wu, K. Elouarzaki, S. Luo, Y. Sun, C. Dai, S. Xi, Y. Chen, X. Lin, M. Fang, X. Wang, D. Mandler and Z. J. Xu, *Sci. Adv.*, 2023, **9**, eadh9487.

41 Q. Yang, C. Zhang, B. Dong, Y. Cui, F. Wang, J. Cai, P. Jin and L. Feng, *Appl. Catal., B*, 2021, **296**, 120359.

42 Y. Liu, S. F. Zhao, S. X. Guo, A. M. Bond, J. Zhang, G. Zhu, C. L. Hill and Y. V. Geletii, *J. Am. Chem. Soc.*, 2016, **138**, 2617–2628.

43 S. G. Bratsch, *J. Phys. Chem. Ref. Data*, 1989, **18**, 1–21.

44 S. C. S. Lai, N. P. Lebedeva, T. H. M. Housmans and M. T. M. Koper, *Top. Catal.*, 2007, **46**, 320–333.

45 H. A. Gasteiger, N. Markovic, P. N. Ross and E. J. Cairns, *J. Phys. Chem.*, 1993, **97**, 12020–12029.

46 D. Y. Chung, K.-J. Lee and Y.-E. Sung, *J. Phys. Chem. C*, 2016, **120**, 9028–9035.

47 S. S. Mahapatra and J. Datta, *Int. J. Electrochem.*, 2011, **2011**, 1–16.

48 A. Yuda, A. Ashok and A. Kumar, *Catal. Rev.*, 2020, 1–103, DOI: 10.1080/01614940.2020.1802811.

49 Y.-W. Zhou, Y.-F. Chen, K. Jiang, Z. Liu, Z.-J. Mao, W.-Y. Zhang, W.-F. Lin and W.-B. Cai, *Appl. Catal., B*, 2021, **280**, 119393.

50 J.-T. Li, Q.-S. Chen and S.-G. Sun, *Electrochim. Acta*, 2007, **52**, 5725–5732.

51 S. X. Liu, L. W. Liao, Q. Tao, Y. X. Chen and S. Ye, *Phys. Chem. Chem. Phys.*, 2011, **13**, 9725–9735.

52 I. Tkach, A. Panchenko, T. Kaz, V. Gogel, K. A. Friedrich and E. Roduner, *Phys. Chem. Chem. Phys.*, 2004, **6**, 5419–5426.

53 C. Wei, R. R. Rao, J. Peng, B. Huang, I. E. L. Stephens, M. Risch, Z. J. Xu and Y. Shao-Horn, *Adv. Mater.*, 2019, **31**, e1806296.

54 D. Xiong, W. Li and L. Liu, *Chem. – Asian J.*, 2017, **12**, 543–551.

55 H. Jiang, Y. Guo, T. Wang, P.-L. Zhu, S. Yu, Y. Yu, X.-Z. Fu, R. Sun and C.-P. Wong, *RSC Adv.*, 2015, **5**, 12931–12936.

56 H. Hu, F. Xie, Y. Pei, M. Qiao, S. Yan, H. He, K. Fan, H. Li, B. Zong and X. Zhang, *J. Catal.*, 2006, **237**, 143–151.

57 M. A. Matin, E. Lee, H. Kim, W.-S. Yoon and Y.-U. Kwon, *J. Mater. Chem. A*, 2015, **3**, 17154–17164.

58 N. R. Babij, E. O. McCusker, G. T. Whiteker, B. Canturk, N. Choy, L. C. Creemer, C. V. D. Amicis, N. M. Hewlett, P. L. Johnson, J. A. Knobelsdorf, F. Li, B. A. Lorsbach, B. M. Nugent, S. J. Ryan, M. R. Smith and Q. Yang, *Org. Process Res. Dev.*, 2016, **20**, 661–667.

59 T. Chatterjee, E. Boutin and M. Robert, *Dalton Trans.*, 2020, **49**, 4257–4265.

60 T. H. M. Housmans, A. H. Wonders and M. T. M. Koper, *J. Phys. Chem. B*, 2006, **110**, 10021–10031.

61 A. Wibowo, N. Chiarasumran, A. Thanapimmetha, M. Saisriyoot, P. Srinophakun, N. Suriyachai and V. Champreda, *Catalysts*, 2022, **12**, 1215.

62 Y. Ahn, J. Byun, D. Kim, B.-S. Kim, C.-S. Lee and J. Han, *Green Chem.*, 2019, **21**, 3442–3455.

63 International Organization for Standardization. Environmental management: life cycle assessment; requirements and guidelines (2005).

64 International Organization for Standardization. ISO 14040-environmental management-life cycle assessment-principles and framework (2006).

65 H. Shin, K. U. Hansen and F. Jiao, *Nat. Sustainability*, 2021, **4**, 911–919.

66 T. R. D. Steward and J. Zuboy, *H2A central production model, version 3 user guide*, National Renewable Energy Laboratory, 2012.

67 M. Jouny, W. Luc and F. Jiao, *Ind. Eng. Chem. Res.*, 2018, **57**, 2165–2177.

68 A. Al-Qahtani, B. Parkinson, K. Hellgardt, N. Shah and G. Guillen-Gosalbez, *Appl. Energy*, 2021, **281**, 115958.

69 Alibaba product search: methanol 99%, category: alcohol & hydroxybenzene & ether, min order: 12 metric tons, https://www.alibaba.com/trade/search?fsb=y&IndexArea=product_en&CatId=&tab=&SearchText=methanol_85%2525, (accessed 2023).

70 Alibaba product search: formic acid 85%, category: organic acid, min order: 10 metric tons, https://www.alibaba.com/products/formic_acid_85%2525.html, (accessed 2023).

71 Today in energy (U.S. Energy Information Administration), https://www.eia.gov/todayinenergy/prices.php, (accessed 2023).

3688 | *Energy Environ. Sci.*, 2025, **18**, 3680–3688

This journal is © The Royal Society of Chemistry 2025